Steven R. Winterstein
e-mail: srw@stanford.edu

Bert Sweetman

Civil and Environmental Engineering Department,
Stanford University,
Stanford, CA 94305

Air Gap Response of Floating Structures: Statistical Predictions Versus Observed Behavior

The air gap response of a specific semi-submersible platform subjected to irregular waves is considered. Detailed model tests for this structure are studied in depth. Using time-histories of both motions and air gap, statistical analyses both for the absolute near-structure wave elevation (with respect to a fixed observer), and the relative wave elevation (with respect to the moving structure) are performed. Statistics of wave crest amplification, due to diffraction, are established. Corresponding amplification factors are derived from linear diffraction theory, and the results of theory and observations are critically compared. [DOI: 10.1115/1.1377867]

Introduction

The air gap response, and potential deck impact, of ocean structures under random waves is generally of considerable interest. While air gap modeling is of concern both for fixed and floating structures, it is particularly challenging in the case of floaters because of their large volume, and the resulting effects of wave diffraction and radiation. These give rise to two distinct effects: 1) global forces and resulting motions are significantly affected by diffraction effects; and 2) the local net wave elevation, $\eta_{\text{net}}(t)$, can also be considerably influenced by diffraction, particularly at locations above a pontoon and/or near a major column. Both effects are important in air gap prediction: we need to know both how high the waves rise, and how low the deck translates vertically (due to net heave and pitch) at a given point to meet the waves. We consider here both effects, but focus primarily on the net wave elevation $\eta_{\text{net}}(t)$—as we believe this to be the most challenging modeling step to predict the air gap response.

We consider in this paper a specific semi-submersible platform, Veslefrikk, which is currently operated by Statoil in the North Sea at a water depth of 574 ft (175 m). Our focus here is to compare detailed model test results with the predictions from linear diffraction theory. Specifically, we have two main goals:

- We seek to demonstrate how the test data can be efficiently analyzed, relating fractiles of the input far-field wave $\eta(t)$ and the output near-structure wave η_{net}. This results in an effective ''crest amplification factor'' for use in air gap design. While applied here specifically to the air gap problem, we believe such a fractile-based approach can be useful in calibrating design wave procedures in a wide range of applications.
- We seek to test the adequacy of linear diffraction analysis. We recognize here that ocean waves are inherently nonlinear, and that this nonlinearity cannot be ignored in predicting statistics of extreme crests. The hypothesis to be tested here, however, is that the main source of nonlinearity lies in the input incident waves, and that the correction in wave crest amplitude due to diffraction can be well-estimated by the corresponding correction predicted by linear theory.

Note that this paper describes ongoing work into the statistical analysis of the air gap problem. In conjunction with studying experimental results directly, statistical post-processing algorithms are currently under development to predict extreme air gap statistics consistent with linear and/or nonlinear diffraction analyses, e.g., [1,2].

Problem Definition

Our test data come from a 1:45-length-scale model of Veslefrikk, tested in the wave tank at Marintek under various types of irregular waves [3]. Figure 1 shows a plan view of the platform, together with the nine, locations for which the air gap responses have been measured as a function of time. As Fig. 1 shows, all tests studied here apply long-crested waves in a diagonal direction with respect to the structure.

Table 1 summarizes the geometric properties of the platform. Tests have been run for two different draft levels: $d=75.5$ ft (23 m) and $d=85.3$ ft (26 m). The cases with deeper draft conform with the original Veslefrikk operating conditions, during which wave impact with the underside of the deck was observed in the field (and reproduced in these model tests). We focus here on the observed results for the more shallow draft, $d=75.5$ ft (23 m).

In the model tank tests, the waves have first been imposed with the model removed, and the incident wave $\eta(t)$ measured at lo-

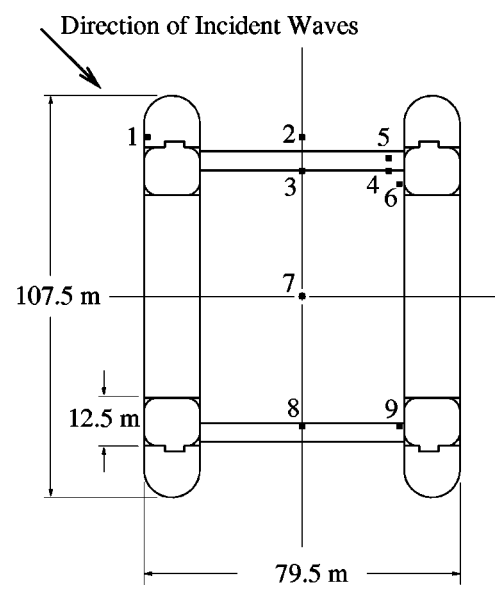

Fig. 1 Plan view of Veslefrikk platform and location of air gap probes

Contributed by the OMAE Division and presented at the 18th International Symposium and Exhibit on Offshore Mechanics and Arctic Engineering, St. Johns, Newfoundland, Canada, July 11–16, 1999, of THE AMERICAN SOCIETY OF MECHANICAL ENGINEERS. Manuscript received by the OMAE Division, March 10, 2000; revised manuscript received March 20, 2001. Associate Editor: A. Naess.

Copyright © 2001 by ASME

Table 1 Characteristics of Veslefrikk platform

Platform Particulars	
Length Over All (LOA):	107.50 m
Longitudinal Column Spacing:	68.00 m
Transverse Column Spacing:	67.00 m
Column Length w/o Sponson:	12.50 m
Column Breadth:	12.50 m
Pontoon Breadth:	14.25 m
Pontoon Height:	9.50 m
Draft, D:	23.00 m
Displacement:	40,692 tonnes
Airgap to Still Water Level:	17.50 m
Center of Gravity (from keel):	24.13 m
Pitch Radius of Gyration:	33.76 m
Roll Radius of Gyration:	34.26 m
Transverse Metacentric Height:	2.36 m
Water Depth:	175.00 m

Table 2 Seastate parameters for which model tests were conducted

H_S [m]	T_P [s]	γ	Number of 3-hour tests
12.0	11.5	4.0	5
14.0	13.5	3.0	6
15.5	16.5	2.0	2

cation 7, where the platform is to be centered. Following common practice, $\eta(t)$ histories have been generated from a stationary random process model, applied over a fixed ''seastate'' duration of $T_{ss}=3$ h. Its spectral density function, $S_\eta(f)$, is described by three basic parameters: 1) the significant wave height $H_S=4\sigma_\eta$, which determines the total spectral power; 2) the peak spectral period T_P, at whose corresponding frequency $f_P=1/T_P$ the spectrum is maximized; and 3) the peakedness factor γ, which determines precisely how narrow (peaked) the spectrum $S_\eta(f)$ is near f_p. There different test conditions were performed for the $d=75.5$ ft(23 m) draft; Table 2 describes the H_S, T_P, and γ values for each of these three test conditions.

Relating Wave Elevation to Air Gap

As noted in the foregoing, it is useful to first consider the net wave elevation, η_{net}, with respect to a fixed origin. The next logical step is to consider the relative wave elevation $r(t)$ measured with respect to the moving structure (e.g., that would be measured by a wavestaff attached to the structure)

$$r(t)=\eta_{\text{net}}(t)-\delta(t) \tag{1}$$

Here, $\delta(t)$ denotes the net vertical displacement at the field point of interest, which in turn is generally a mixture of the form

$$\delta(t)=\xi_3(t)+y\cdot\xi_4(t)-x\cdot\xi_5(t) \tag{2}$$

in terms of the rigid-body motions ξ_3, ξ_4, and ξ_5 in heave, roll, and pitch, and the field-point location (x,y) of interest. Finally, the available air gap $a(t)$ is the difference between the still-water air gap, a_0, and the relative wave $r(t)$

$$a(t)=a_0-r(t) \tag{3}$$

In the following we shall focus mainly on $\eta_{\text{net}}(t)$, which is likely the most challenging quantity to model, and then on the relative wave elevation $r(t)$—and hence, by implication, the air gap response $a(t)$. Note, however, that we infer these quantities from measurements in the inverse order; that is, air gap probes directly measure $a(t)$, from which we use Eq. (3) to infer $r(t)$, and Eqs. (1)–(2) to infer $\delta(t)$, and hence $\eta_{\text{net}}(t)$. (The test results include measurements of the motions ξ_i in all 6 degrees of freedom.)

Crest Amplification From Data Analysis

In a design wave approach, it is common to consider the consequence of a single incident wave cycle, with critical values of amplitude and associated period and profile. The resulting critical response level during this cycle is then taken as the basis for design procedures, generally with appropriate load factors; e.g., [4]. We consider here the use of a similar cycle-by-cycle analysis to predict extreme values of the net wave η_{net}, and also of the relative wave $r(t)$ with respect to the structure.

Cycle-by-Cycle Results From Concurrent Data. In establishing appropriate calibration factors for a design wave approach, it is common to seek a relationship between the input and output amplitude in *concurrent* cycles. Specifically, from the input wave process $\eta(t)$ we define ''cycles'' as periods separated by successive upcrossings of the mean level $m_\eta=0$. The input wave amplitudes $X_1\ldots X_N$ are then the peak (crest) amplitudes for each cycle of $\eta(t)$, and the response amplitudes $Y_1\ldots Y_N$ are the corresponding maximum values of the response (here, η_{net}) occurring during each of the N input wave cycles.

One may then seek to use linear regression to relate the amplitudes X_i and Y_i of the input and output wave

$$Y_i=a_c+b_cX_i+\epsilon \tag{4}$$

The subscript c is used here to indicate that one is trying to predict the output wave amplitude Y_i as a function of the concurrent input amplitude X_i in the same cycle. Regression estimates then yield the parameter estimates

$$b_c=\rho\frac{\sigma_Y}{\sigma_X};\quad a_c=m_Y-b_cm_X;\quad \sigma_\epsilon^2=(1-\rho^2)\sigma_Y^2 \tag{5}$$

in terms of the estimated (sample) means m_X and m_Y of X and Y, the corresponding variances σ_X^2 and σ_Y^2, and the correlation coefficient ρ between X and Y. Note that these statistics are the means, variances and correlation coefficient of the peaks of the processes, and not of the entire processes. These rms peak values reflect the nonlinear nature of the extremes to a greater extent than the rms of the process, which only weakly reflects nonlinear effects [5].

To illustrate, we focus first on the seastate with parameters $H_S=45.9$ ft (14.0 m), $T_P=13.5$ s, for which most data are available ($T=3$ h$\times 6$ tests$=18$ h). Concatenating these tests yields a total of $N=5422$ input wave cycles. Figures 2–4 show the resulting $N=5422$ (X_i,Y_i) data corresponding to output waves η_{net} at locations 7, 5, and 1, respectively. (The input waves are the same, hence only the Y_i values differ in these figures.) Recall from Fig. 1 that location 7 corresponds to the platform center, while locations 1 and 5 are just in front of major columns. As may be expected, the near-column locations show somewhat larger maximum crest levels: $Y_{\max}$, is roughly 66 ft (20 m at location 5 and 82 ft (25 m) at location 1, compared with an input maximum $X_{\max}$ of roughly 59 ft (18 m).

To characterize this amplification statistically, Figs. 2–4 also show the mean trend $a_c+b_cX_i$ from linear regression. (The other

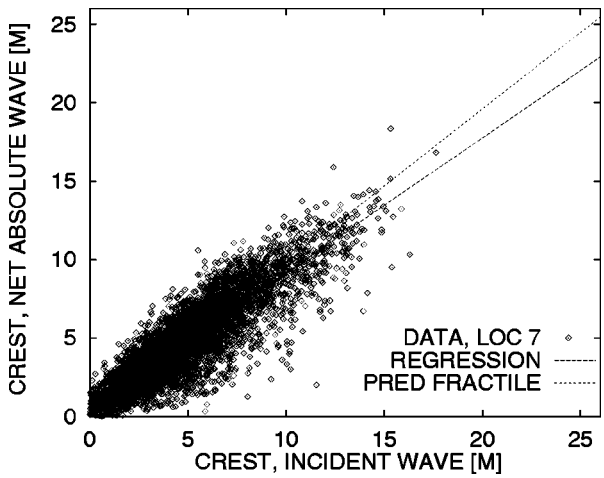

Fig. 2 Concurrent crest data; location 7 (platform center)

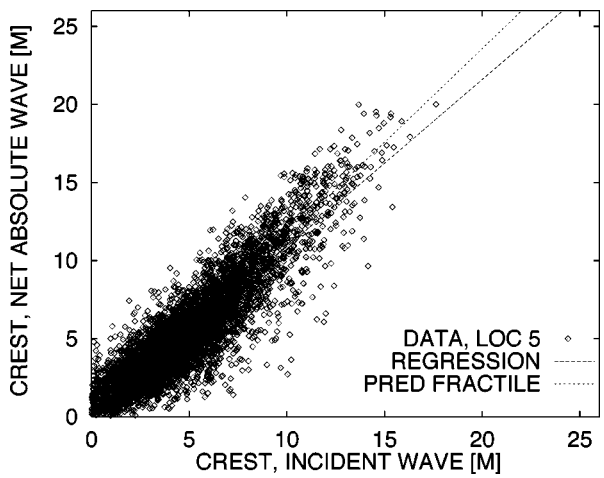

Fig. 3 Concurrent crest data; location 5

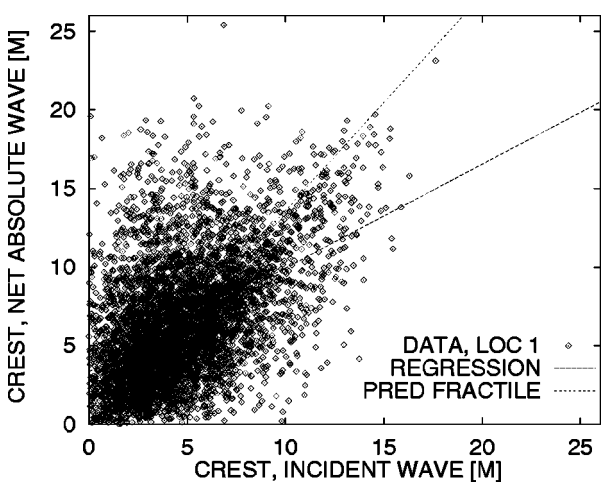

Fig. 4 Concurrent crest data; location 1

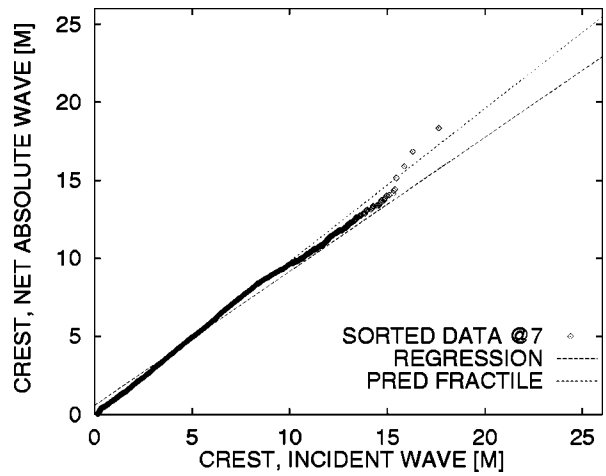

Fig. 5 Ordered (fractile) crest data; location 7 (platform center)

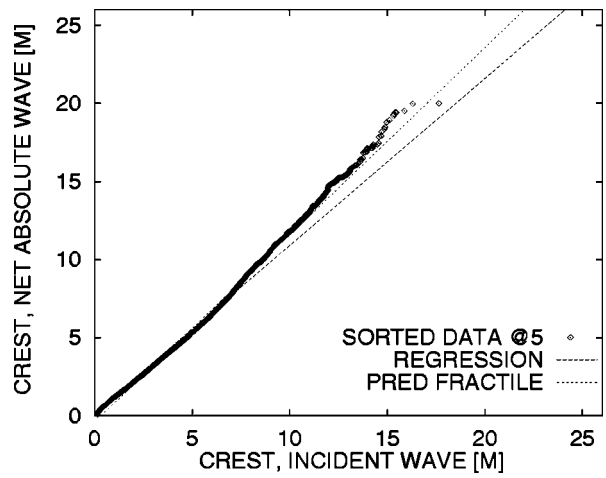

Fig. 6 Ordered (fractile) crest data; location 5

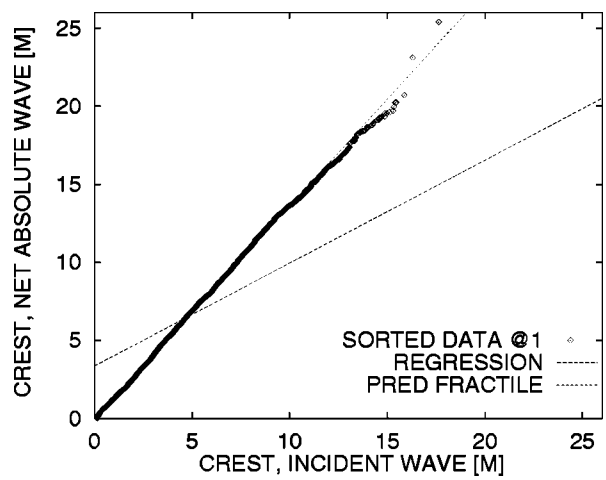

Fig. 7 Ordered (fractile) crest data; location 1

lines shown, which predict fractiles of y, will be explained later in connection with Figs. 5–7.) Note the following difficulties with using the regression trend only:

• Because the mean trend line neglects the effect of the ε term in Eq. (4), it will generally underestimate the marginal variability of Y. Indeed, in the limit as $\rho \rightarrow 0$, we will generally find a horizontal trend ($b_c \rightarrow 0$), regardless of how high the marginal variability σ_Y becomes with respect to σ_X. As a result, we often find here that $b_c < 1$, despite the fact that extreme Y values are generally larger than corresponding X values. (For convenience of visual comparison, note that all figures have identical X and Y

scales; hence a ''neutral'' slope $b=1$ would connect the lower-left and upper-right vertices of the figure window.) Note especially the results for location 1 (Fig. 4): the regression slope is found to be only $b_c=0.66$, despite the fact that extreme Y outcomes appear systematically larger than corresponding extreme X values.

• The relatively small slope value b_c in Eq. (5) arises from the goal of standard regression, which is to minimize errors in predicting Y_i for given X_i. One may instead seek a best prediction of X_i for given Y_i; this yields a steeper line, with slope $b_c' = dY/dX = (1/\rho)\cdot\sigma_Y/\sigma_X$. This, however, neglects the corresponding variability of X at given Y, thereby giving a systematically low dX/dY, and hence high dY/dX.

• We may seek other, modified versions of regression analyses that produce ''more reasonable'' trends. Fundamentally, however, one may question the adequacy of any single trendline, when based on data as scattered as in Fig. 4. We show in the forthcoming how such regression results can still be used in a design-wave approach, even when the data show such large cycle-to-cycle variability as in Fig. 4.

Fractile Results From Ordered and Nonordered Data. For design of structures against extreme waves, one is often most interested not in the response Y_i in a specified wave cycle i, but rather in the response level Y_p with a specified exceedance probability p. If we have a corresponding estimate of the input wave amplitude X_p at the same probability level, we may seek a new, deterministic linear relation between X_p and Y_p directly

$$Y_p = a_p + b_p X_p \tag{6}$$

Note that the notation a_p and b_p for these coefficients is intended to denote that the resulting trend is intended to apply on a fractile-by-fractile basis (i.e., for given p). In contrast, a_c and b_c have been derived from a concurrent basis (i.e., for given wave cycle i, or alternate choices of concurrent input/output ''events'').

We may seek to estimate the coefficients a_p in b_p in Eq. (6) directly from the reprocessed data, in which X_p is plotted versus Y_p. Effectively, this amounts to reordering both the X_i and Y_i data vectors; for example, the largest X_i and Y_i value are both assigned the same fractile level $p=1/N$, the second largest values $p=2/N$, and so forth. Alternatively, we suggest here a simpler way to directly predict the parameters a_p and b_p without reordering data—which can be inferred directly from the statistics of cycle-by-cycle data. In particular, if we assume that X_i and Y_i each have marginal normal probability distributions, we may write

$$\frac{Y_p - m_Y}{\sigma_Y} = \frac{X_p - m_X}{\sigma_X} = U_p \tag{7}$$

in which U_p is the corresponding fractile of a *standard* normal distribution (e.g., $U_p=0.0$ for $p=0.5$, $U_p=1.0$ for $p=0.84$, etc.). Each statistical quantity expressed in Eq. (7) refers to just the peaks of the process, rather than to the process itself. One may rewrite the equation in the form of Eq. (6), in which the trendline parameters are simply

$$b_p = \frac{\sigma_Y}{\sigma_X} = \frac{b_c}{\rho}; \quad a_p = m_Y - b_p m_X \tag{8}$$

Note that Eqs. (7)–(8) are not restricted to the Gaussian distribution model. They apply to any distribution that has an additive shift parameter and a multiplicative scale parameter; common examples include both the Gumbel and Gaussian distributions. For some other distributions, such as the Weibull and lognormal, this assumption should be applied to $\ln(Y)$ versus $\ln(X)$. The choice of distributions can be dictated by the appearance of the data as plotted on linear or on log scales. The air gap results presented in Figs. 5–7 plot as nearly straight lines on the linear scale shown.

Figures 5–7 show that this simple predicted fractile line, with $b_p=\sigma_Y/\sigma_X$, generally agrees quite well with the observed, ordered (X_p, Y_p) data. Note that this agreement holds even at location 1 (Fig. 7), despite the significantly scattered cycle-by-cycle data (Fig. 4) on which it is based. This suggests that we can predict the fractile trendline from Eq. (6) without reordering the data, in one of two ways:

- $b_p = b_c/\rho$; i.e., inflating the regression slope b_c by a factor of $1/\rho$.
- $b_p = \sigma_Y/\sigma_X$, the ratio between the standard deviations of the Y and X. This avoids the regression analysis of paired data.

Note that this fractile trendline is preserved if the roles of X and Y are interchanged; in this case $dX/dY = \sigma_X/\sigma_Y$, and hence $b_p = dY/dX$ remains equal to σ_Y/σ_X. Note also that like both mean regression lines (of Y given X and vice versa), the line relating Y_p to X_p from Eqs. (6) and (8) also passes through the mean pair (m_X, m_Y) from the data. At all other points, Eq. (6) passes between these two regression trends, in view of its intermediate slope.

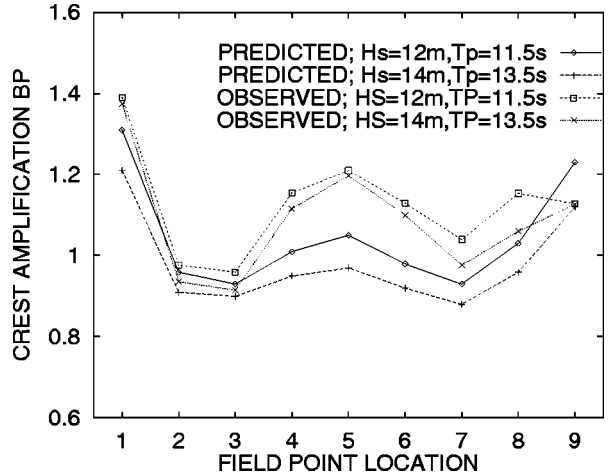

Fig. 8 Theory versus data: absolute wave amplification

Results Across Field Points. The foregoing suggests that the slope b_p, from Eq. (8), serves as a useful ''response amplification factor,'' relating input and output levels at corresponding fractiles. (Note that a_p is found to be nearly zero here; i.e., the predicted fractile lines in Figs. 5–7 nearly pass through the origin.) The ''OBSERVED'' results in Fig. 8 shows the resulting crest amplification factors, b_p, found for all field points from the two sea-states with most data: $(H_S, T_P) = (39.4\text{ ft}, 11.5\text{ s}) = (12\text{ m}, 11.5\text{ s})$ and $(45.9\text{ ft}, 13.5\text{ s}) = (14\text{ m}, 13.5\text{ s})$. The largest observed amplification, roughly 1.4, is found at location 1 (in front of the up-wave column). Other near-column locations (4, 5, 6, and 9) show amplification factors of roughly 1.2. As might be expected, somewhat greater amplifications generally occur for the smaller T_P case (with shorter wavelengths, hence larger relative effect of the structure). The largest amplifications, however, at the near-column locations are relatively constant for the two T_P cases considered. The corresponding predicted results in Fig. 8 are described in the forthcoming.

Crest Amplification From Diffraction

Formally, we may split the input incident wave $\eta(t)$ into a ''linear part'' $\eta_L(t)$ and a remaining ''nonlinear contribution'' $\eta_{NL}(t)$

$$\eta(t) = \eta_L(t) + \eta_{NL}(t) \tag{9}$$

While $\eta(t)$ describes the actual wave surface, $\eta_L(t)$ describes our linear approximation in solving its governing equations (i.e., imposing the free-surface condition at the still water level, rather than at the actual time-varying surface). The nonlinear term

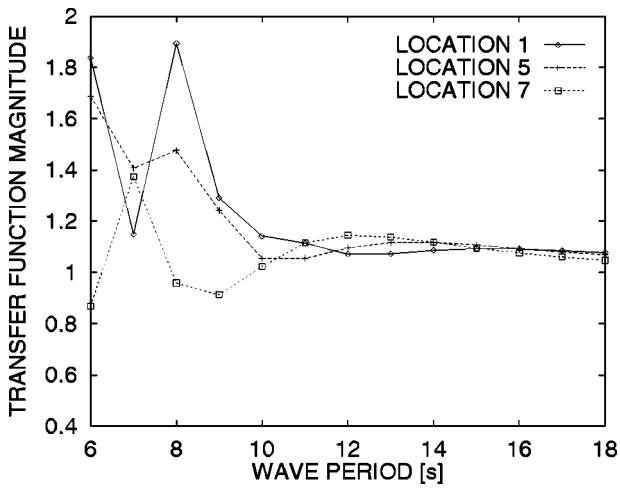

Fig. 9 $|H_{\text{net}}(T)|$ = amplitude of transfer function from input undisturbed wave to output net wave η_{net} in the presence of the structure. Predictions are from first-order diffraction analysis.

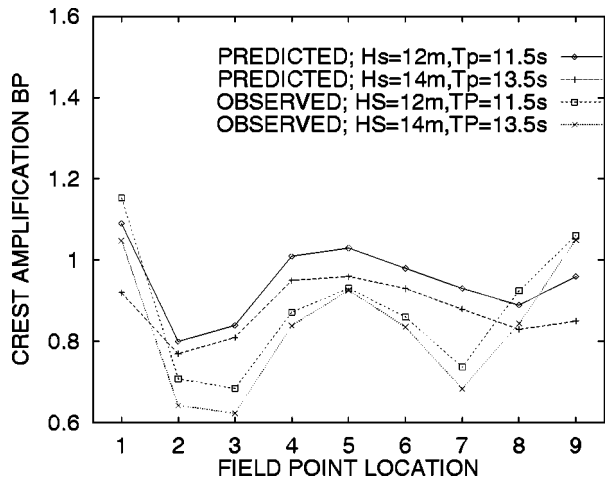

Fig. 10 Theory versus data: relative wave amplification

$\eta_{NL}(t)$ is thus defined implicitly, as the difference between $\eta(t)$ and $\eta_L(t)$. In fact, detailed statistical studies suggest that $\eta_{NL}(t)$ is often accurately predicted by a second-order, random wave model [6].

In a similar way, we may decompose the net ''output'' near-structure wave, $\eta_{\text{net}}(t)$, into linear and remaining nonlinear terms

$$\eta_{\text{net}}(t) = \eta_{\text{net},L}(t) + \eta_{\text{net},NL}(t) \tag{10}$$

Linear diffraction codes, e.g., [7], estimate the transfer function, $H_{\text{net}}(f)$ that relates $\eta_L(t)$ to $\eta_{\text{net},L}(t)$ at a given wave frequency f. Figure 9 shows the transfer function amplitude, $|H_{\text{net}}|$, as a function of wave period $T=1/f$, for a selected set of field points. As expected, results across field points converge in the long-wave, large-T limit. Significant differences are predicted, however, at smaller periods: at $T=8$ s$|H_{\text{net}}|$ varies from 1.0 at location 7 (mid-platform), to 1.9 and 1.5 at the near-column locations 1 and 5.

To consider the consequence of sampling this transfer function according to a given wave spectrum $S_\eta(f)$, we consider the amplification factor b_{RMS} in the RMS value predicted by linear theory

$$b_{\text{RMS}} = \frac{\sigma_{\eta_{net}}}{\sigma_\eta} = \left[\frac{\int_0^\infty |H_{\text{net}}(f)|^2 S_\eta(f)\,df}{\int_0^\infty S_\eta(f)\,df} \right]^{1/2} \tag{11}$$

The resulting values of b_{RMS} are shown as the ''PREDICTED'' results in Fig. 8. (Note again that our hypothesis here is not that the linear model will yield the correct extreme value of either η or η_{net}, but merely that it can yield a useful estimate of the correction factor between them.) In fact the predictions show the same general trends as the observations: larger results at the near-column locations and in the smaller-T_P seastate. Amplification levels are somewhat underpredicted at several near-column locations: at location 1, $b_{\text{RMS}}=1.2-1.3$ compared with an observed $b_p=1.4$, while $b_{\text{RMS}}=0.9-1.0$ at locations 4, 5, 6 compared with $b_p=1.1-1.2$ from the observed data. These additional amplifications may be the result of nonlinear diffraction, or may represent near-column effects beyond the realm of a conventional diffraction analysis.

Finally, Fig. 10 shows similar results for the relative wave elevation, $r(t)$, with respect to the moving structure. Because the structure generally moves with the waves, the relative wave is generally less than the absolute wave level, yielding factors in Fig. 10 that are generally lower than in Fig. 8. ''OBSERVED'' results in Fig. 10 again predict b_p as in Eq. (8), now treating $r(t)$ as the relevant response history. ''PREDICTED'' results in Fig. 10 again use Eq. (11), now with a transfer function $H_r(f)$ to the relative motion described in Eqs. (1)–(2), which include the (linear) predicted transfer functions for heave, pitch, and roll. Again, the predictions are found to show a similar trend to the observed behavior. The most striking difference now occurs at field points near the platform center in the along-wave direction (locations 4, 5, 6, 7), whose vertical motion δ is dominated by heave rather than pitch or roll. Our predictions here overestimate the relative wave elevation, suggesting that they underestimate the platform heave motion.

The heave motion measured in the model basin has been spectrally analyzed and is presented in Fig. 11. The first-order predicted spectrum of heave motion (shown in the figure as ''PREDICTED'') has been calculated using only the first-order transfer functions from linear diffraction. The spike that can be observed in the measured spectrum, at about 0.045 Hz, coincides with the heave natural frequency of the vessel. The analysis omits this resonant effect, as no model of slow drift motions was available. Inclusion of the effects of vessel motion in the statistical analysis is straightforward [2], and is a topic of ongoing study.

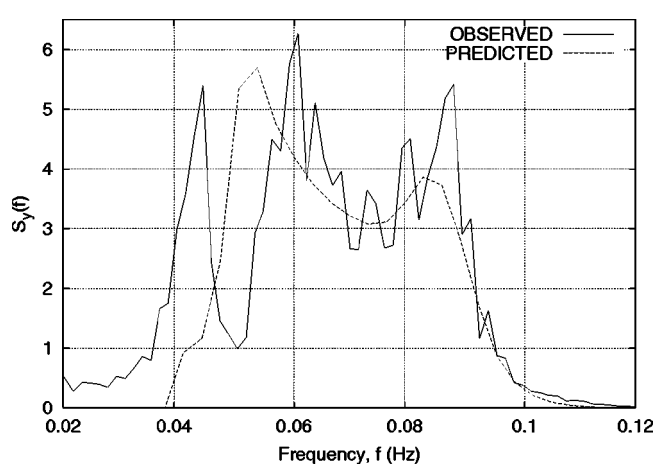

Fig. 11 Comparison of observed and predicted heave motion spectra

Summary and Conclusions

• A new, fractile-based approach has been proposed to define an amplification factor, b_p, on extreme wave crest levels due to diffraction. This is calculated as the rms-ratio between input and output peaks in all wave cycles (Eq. (8)). The scaling factor resulting from this new approach is found to describe the output fractile results quite well, even at extreme levels within the 18 h of seastate test results, e.g. Figs. 5–7.

• Figure 8 shows that the largest observed amplification, roughly 1.4, is found at location 1 (in front of the up-wave column; see Fig. 1). Other near-column locations (4, 5, 6, and 9) show amplification factors of roughly 1.2. As might be expected, somewhat greater amplifications generally occur for the smaller T_P case (with shorter wavelengths, hence larger relative effect of the structure). The largest amplifications, however, at the near-column locations are relatively constant for the two T_P cases considered.

• An analogous amplification factor, b_{RMS}, has been defined based on *linear* diffraction theory (Eq. (11)). Note that we seek here to use the linear model not to predict extreme values of of either η or η_{net}, but merely their ratio. In practice, we would propose to apply the correction factor b_{RMS} to a second-order random model of η, for which analytical estimates of extreme fractiles are available [6].

• Numerical results for b_{RMS} show the same general trends as the observations: larger results at the near-column locations and in the smaller-T_P seastate. Amplification levels are somewhat underpredicted at several near-column locations: at location 1, $b_{\mathrm{RMS}} = 1.2-1.3$ compared with an observed $b_p = 1.4$, while $b_{\mathrm{RMS}} = 0.9-1.0$ at locations 4,5,6 compared with $b_p = 1.1-1.2$ from the observed data. These additional amplifications may be the result of nonlinear diffraction, or may represent near-column effects beyond the realm of a conventional diffraction analysis.

Acknowledgments

Financial support for this work has been provided by the National Science Foundation through the Offshore Technology Research Center (Grant CDR-8721512), and by the Office of Naval Research (Grant N0014-9610641). The authors gratefully acknowledge Statoil for supplying the model test data for the Veslefrikk platform, and Aker Engineering for supplying the corresponding diffraction analysis results.

References

[1] Ude, S., Kumar, T. C., and Winterstein, S., 1995, ''TFPoP 2.0: Stochastic Response Analysis of Floating Structures Under Wind, Current, and Second-Order Wave Loads,'' Tech. Rep. RMS-18, Reliability of Marine Structures.

[2] Manuel, L., and Winterstein, S., 1998, ''Estimation of Airgap Statistics for Floating Structures,'' Tech. Rep. TN-4, Reliability of Marine Structures.

[3] Fokk, T., 1995, ''Veslefrikk B Air Gap Model Tests,'' Tech. Rep. 512167.00.01, MARINTEK Trondheim, Norway.

[4] American Petroleum Institute, 1993. *Recommended Practice for Planning, Designing and Constructing Fixed Offshore Platforms—Load and Resistance Factor Design 2A-LRFD (RP 2A-LRFD)*, 1st Edition.

[5] Stansberg, C. T., 1999, ''Nonlinear Air-Gap System Identification from Model Tests,'' *Proc., 9th ISOPE Conference*. Brest, France.

[6] Jha, A. K., 1997, ''Nonlinear Stochastic Models for Loads and Responses of Offshore Structures and Vessels,'' Ph.D. thesis, Stanford University, Stanford, CA.

[7] WAMIT 4.0, 1995. *WAMIT: A Radiation-Diffraction Panel Program for Wave-Body Interactions-User's Manual*. Department of Ocean Engineering, M.I.T., Cambridge, MA.